Supporting Information

Ce-induced NiS Bifunctional Catalyst Transformation: Enhancing Urea Oxidation Coupled with Hydrogen Electrolysis

Yingzhen Zhang [1a,b,c], Wei Zhang [1a], Jianying Huang [a], Weilong Cai [a,b*] and Yuekun Lai [a,b*]*

[a] National Engineering Research Center of Chemical Fertilizer Catalyst (NERC-CFC), College of Chemical Engineering, Fuzhou University, Fuzhou 350116, P. R. China

[b] Qingyuan Innovation Laboratory, Quanzhou 362801, P. R. China

[c] School of Chemistry, Chemical Engineering and Biotechnology, Nanyang Technological University, Singapore 637459, Singapore

[1] These authors contributed equally to this work.

*Corresponding authors: yklai@fzu.edu.cn; wlcai@fzu.edu.cn; jyhuang@fzu.edu.cn

Calculation of reaction activation energy

The apparent electrochemical activation energy (Ea) for UOR and OER can be determined using the Arrhenius relationship[1]:

$$\frac{\partial(logi_k)}{\partial\left({}^{1}/_{T}\right)}|_{\eta} = \frac{E_a}{2.3R} \#(1)$$

where i_k is the kinetic current at a potential of 1.80 V *vs.* RHE, T is the temperature (K), and R is the universal gas constant.

Calculation of Faradaic efficiency for UOR

The Faradic efficiency (FE, %) of the fabricated electrodes for UOR is calculated based on following equations[2-6]:

$$FE = \frac{I_{UOR}}{I} \times 100\% \#(2)$$

$$I = I_{UOR} + I_{OER} \#(3)$$

where, I is the current recorded at each potential step in the presence of urea, I_{OER} is the current acquired without urea. I_{UOR} is the current originated from urea oxidation.

Calculation of Faradaic efficiency for HER

The Faraday efficiency (FE, %) of the H_2 can be determined by the following equation[7]:

$$FE = \frac{N \times Z}{Q} \times F \times 100\% \#(4)$$

where N is the mole of product H_2 roduced, Z is the number of electrons transferred for a mole of H_2 (Z = 2), Q is the passed charge, and F is the Faraday constant (96 485 C mol^{-1}).

Experimental

Reagents and chemicals

Nickel sulfate hexahydrate ($NiSO_4 \cdot 6H_2O$, AR), cerium nitrate hexahydrate ($Ce(NO_3)_3 \cdot 6H_2O$, ≥ 99.95%) was obtained from Aladdin and Macklin, respectively. Urea ($CO(NH_2)_2$, AR), potassium hydroxide (KOH, AR) and thiourea ($CS(NH_2)_2$, AR) was obtained from Sinopharm Chemical Reagent Co., Ltd. Carbon cloth (W0S1011) was brought from Taiwan Carbon Technology Co., Ltd. Ultrapure water was purified through a Millipore Direct-Q 3 water purification system (18.2 MΩ cm^{-1}). All the reagents and chemicals were used without any further purification.

Synthesis of Ce-NiS dual-functional catalyst

The Ce-doped nickel sulfide was grown *in-situ* on the carbon cloth substrate. 1.94 mmol $NiSO_4 \cdot 6H_2O$, 0.06 mmol $Ce(NO_3)_3 \cdot 6H_2O$, and 2 mmol $CS(NH_2)_2$ were dissolved in 40 mL ultrapure water as the electrolyte. The electrodeposition process adopts a typical three-electrode system, in which carbon cloth (1 × 2 cm^2), platinum wire, and Ag/AgCl electrode were used as the working electrode, opposite electrode, and reference electrode, respectively. The Ce-NiS electrocatalyst was synthesized by cyclic voltammetry (CV) method, at the potential range of -1.2-0.2 V *vs.* Ag/AgCl, with a scanning rate of 10 mV s^{-1}. After electrodeposition, the sample was rinsed with ultrapure water and then vacuum dried at 60 °C for 12 h. Under the condition that the volume of ultrapure water and the amount of $CS(NH_2)_2$ were not changed, the total molar amount of metal elements was controlled at 2 mmol, and samples with different doping amounts were prepared by adjusting the molar ratio of $NiSO_4 \cdot 6H_2O$ and $Ce(NO_3)_3 \cdot 6H_2O$.

Electrochemical measurement

The electrocatalytic performance of the as-prepared catalyst was tested on the Versa STAT 3 (Advanced Measurement Technology Inc.) electrochemical workstation. The as-prepared sample, graphite rod, and Hg/HgO electrode were used as the working electrode, opposite electrode, and reference electrode, respectively. The UOR test was carried out in a mixed electrolyte with 0.33 M urea under alkaline conditions (1.0 M KOH, pH = 14). The polarization curve was obtained by linear sweep voltammetry (LSV) method with a scan rate of 5 mV s^{-1}. CV was used to measure the double-layer capacitance (C_{dl}) of the as-synthesized samples, and the electrochemical active surface area (ECSA) was further calculated by the equation[8]: ECSA = C_{dl}/C_s, where C_s was the specific capacitance of the catalyst under alkaline condition. The stability of the electrocatalyst was evaluated by chronoamperometry at 1.45 V *vs.* RHE. All measured potentials ($E_{Hg/Hgo}$) were converted to reversible hydrogen electrode potentials (RHE) by Nernst equation[9] ($E_{RHE}=E_{Hg/Hgo} + 0.0591 \times pH + 0.098$). All measurements were recorded at room temperature.

Characterization

The morphology and composition of the samples were studied by scanning electron microscopy (SEM) of Zeiss Sigma 30. Transmission electron microscopy (TEM) images of electrocatalysts were obtained on a FEI Tecnai G2 F20 S-Twin at an accelerating voltage of 200 kV. The crystalline phases were analyzed by X-ray diffraction (XRD, X'Pert3 Powder diffractometer using Cu Kα radiation). The valence states of elements were analyzed by X-ray photoelectron spectroscopy (XPS, Thermo Scientific K-Alpha spectrometer. The defect of as-prepared samples was gathered by Electron paramagnetic resonance spectroscopy (EPR,

JEOL JES-FA200 instrument). Electrochemical *in-situ* Raman spectroscopy was used to detect the reconfiguration behavior of the catalyst in the electrochemical process by Renishaw in the reflex microscope with a 532 nm laser. The water contact angle of samples was determined by an integrated digital goniometer (OCA25, Dataphysics Instruments Co., Ltd., Germany).

Supplementary Figures

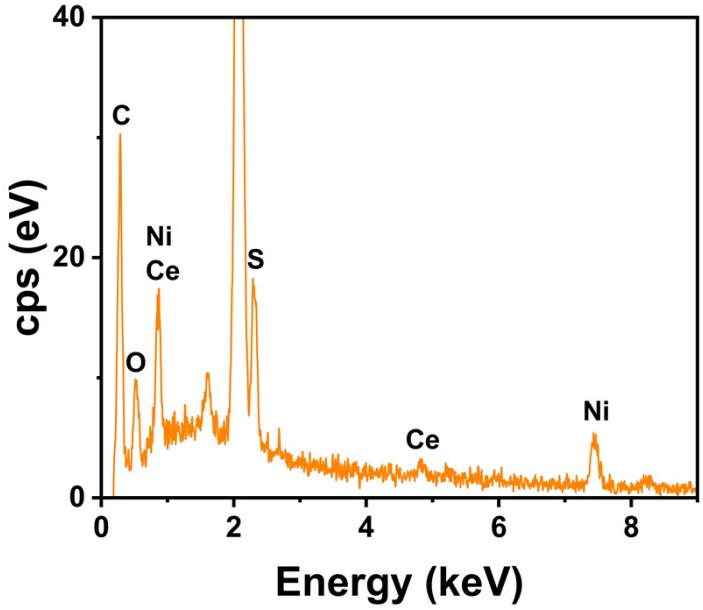

Figure S1. The EDS spectrum of Ce-NiS.

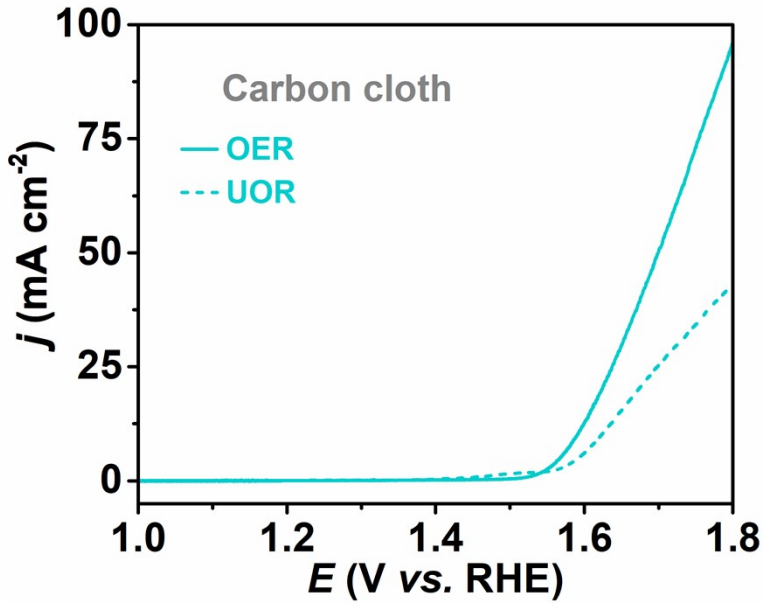

Figure S2 LSV curves of carbon cloth in 1.0 M KOH electrolyte with or without 0.33 M urea.

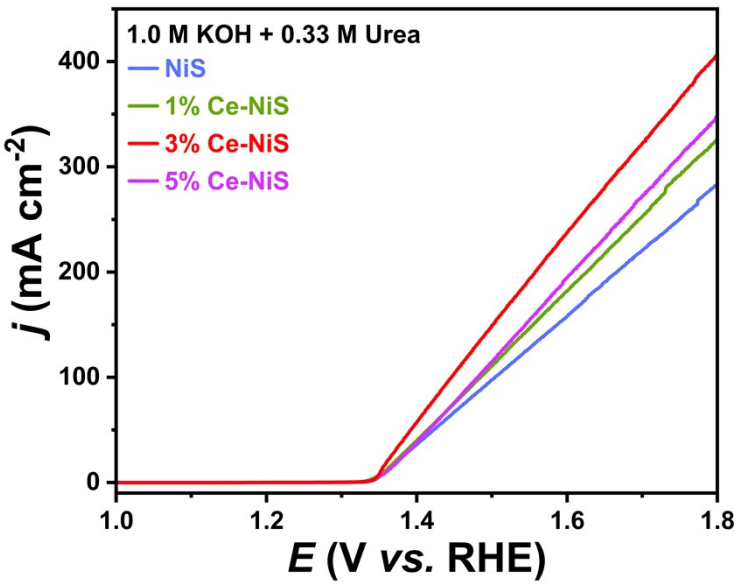

Figure S3. LSV curves of pure NiS and various Ce-doped NiS towards UOR in 1.0 M KOH electrolyte with 0.33 M urea.

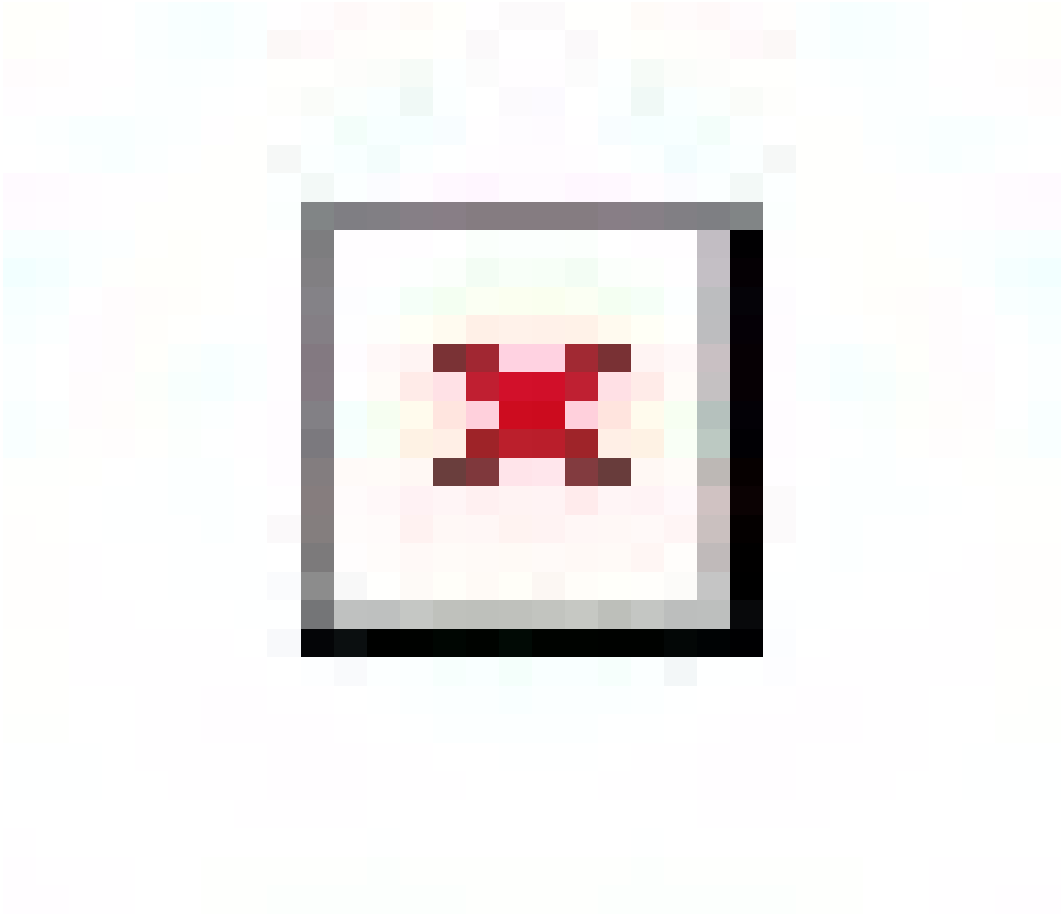

Figure S4. (a) ECSA values and corresponding CV curves at different scan rate (20~200 mV s^{-1}) of (b) Ce-NiS, (c) pure NiS and (d) pure Ce.

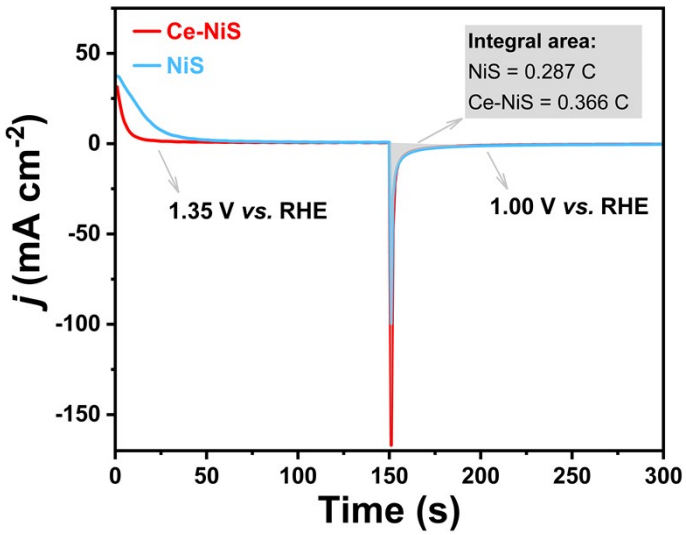

Figure S5. Pulsed chronoamperometry curves of pure NiS and Ce-NiS by oxidization of the electrocatalyst at 1.35 V *vs.* RHE in 1.0 M KOH, followed by reduction at 1.00 V *vs.* RHE.

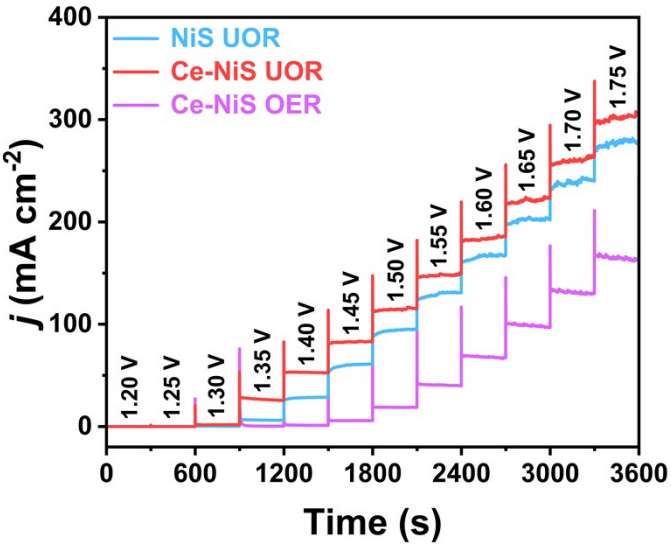

Figure S6. I-t curves of Ce-NiS towards UOR and OER, NiS towards UOR at different potentials (V *vs.* RHE) in differential pulse voltammetry.

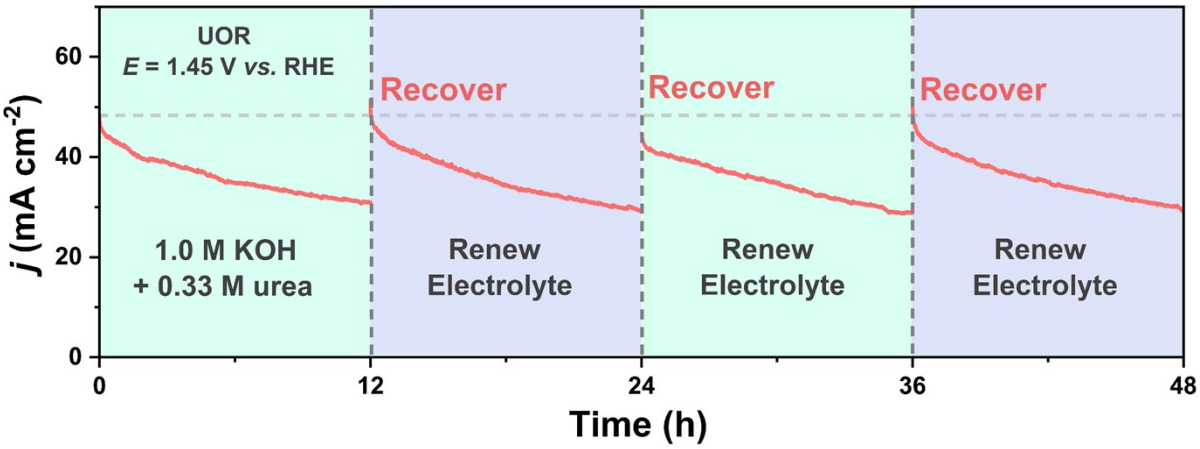

Figure S7. *I*-t curve of Ce-NiS at 1.45 V vs. RHE.

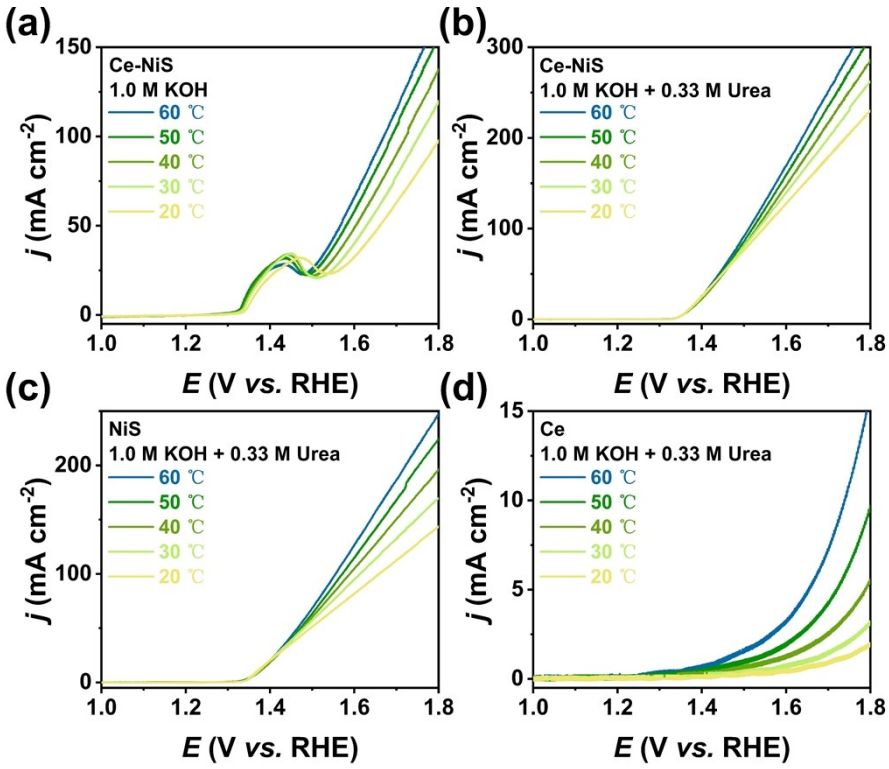

Figure S8. (a) LSV curves of pure Ce-NiS towards OER at various temperature in 1.0 M KOH electrolyte. LSV curves of (b) Ce-NiS, (c) pure NiS and (d) pure Ce towards UOR at various temperature in 1.0 M KOH electrolyte with 0.33 M urea.

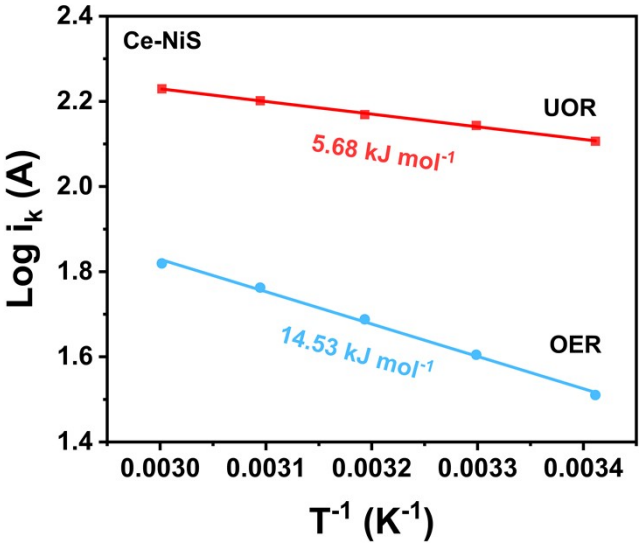

Figure S9. Activation energy of Ce-NiS towards UOR and OER.

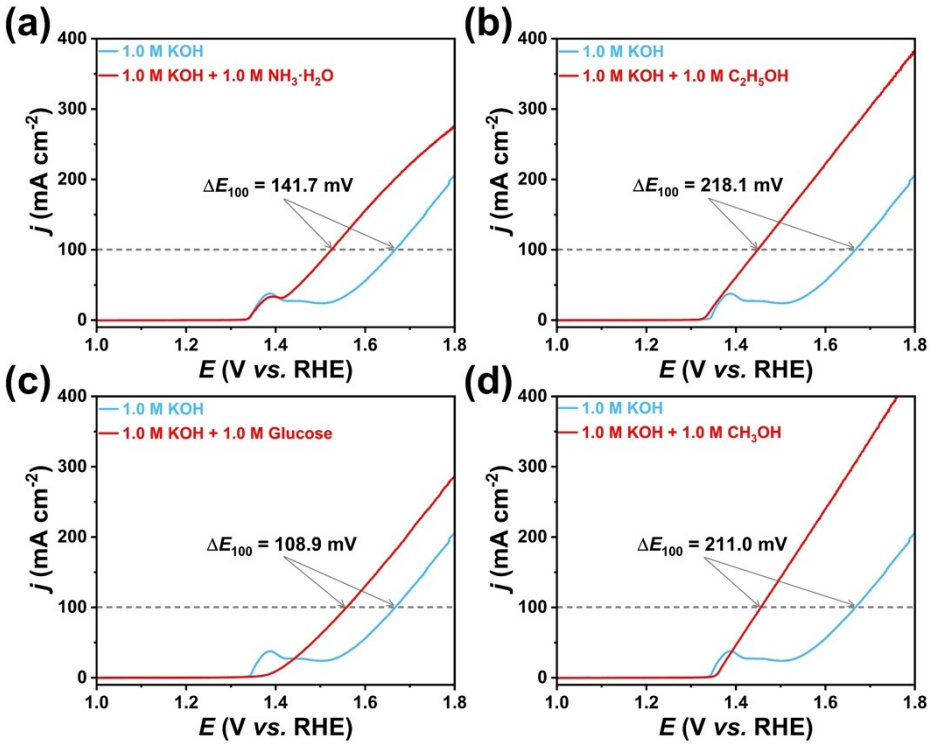

Figure S10. LSV curves of Ce-NiS in 1.0 M KOH electrolyte with 1.0 M (a) C_2H_5OH, (b) CH_3OH, (c) glucose, (d) $NH_3 \cdot H_2O$.

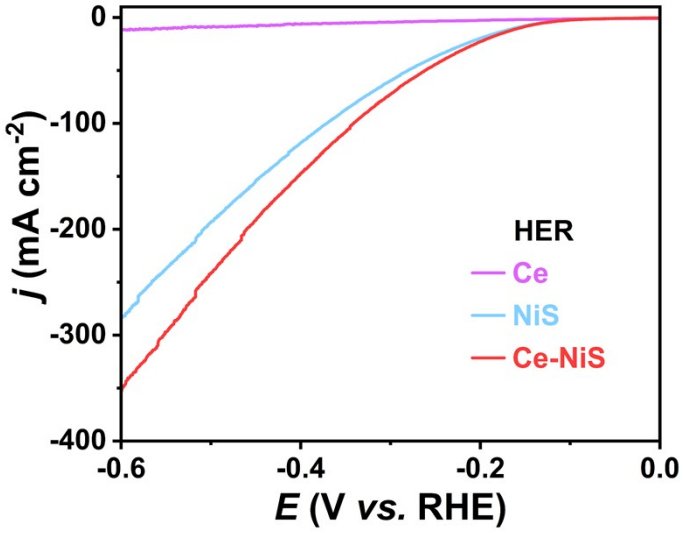

Figure S11. LSV curves of Ce, NiS, and Ce-NiS towards HER in 1.0 M KOH with 0.33 M urea.

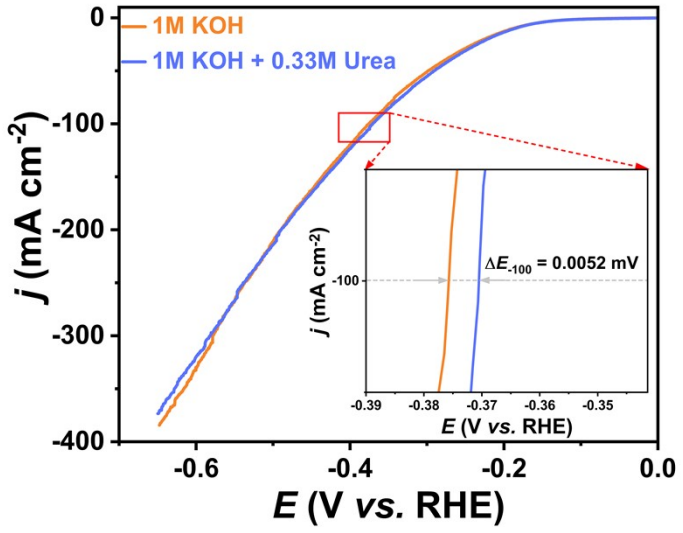

Figure S12. LSV curves of Ce-NiS towards HER in 1.0 M KOH electrolyte with and without 0.33 M urea.

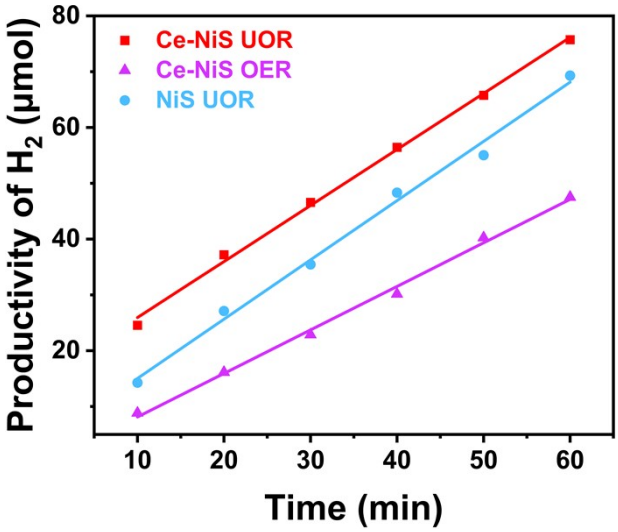

Figure S13. Hydrogen production of Ce-NiS and pure NiS towards OER and UOR.

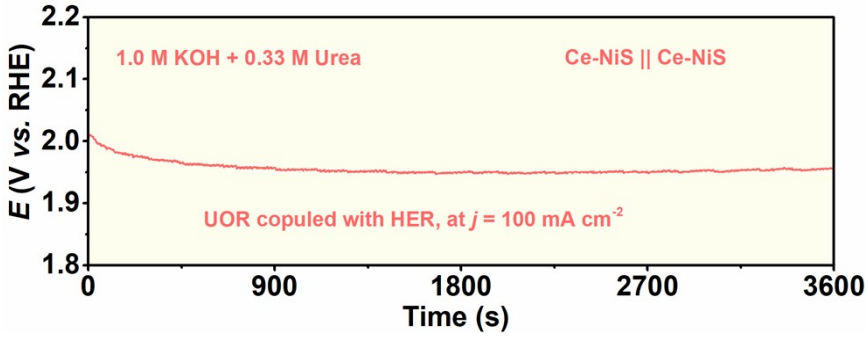

Figure S14. Long-term stability tests at a constant current density of 100 mA cm^{-2} for the Ce-NiS as the as the anodic electrode and cathodic electrode, respectively.

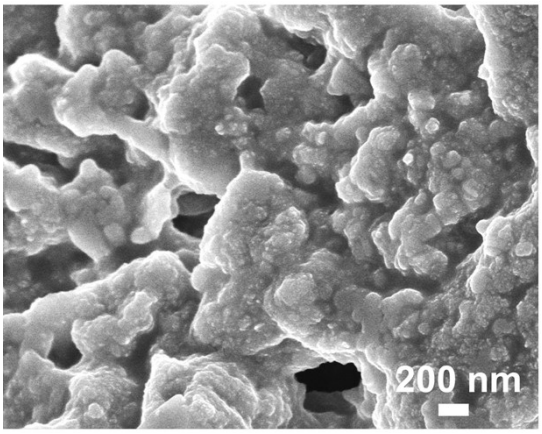

Figure S15. SEM image of Ce-NiS after UOR durability test.

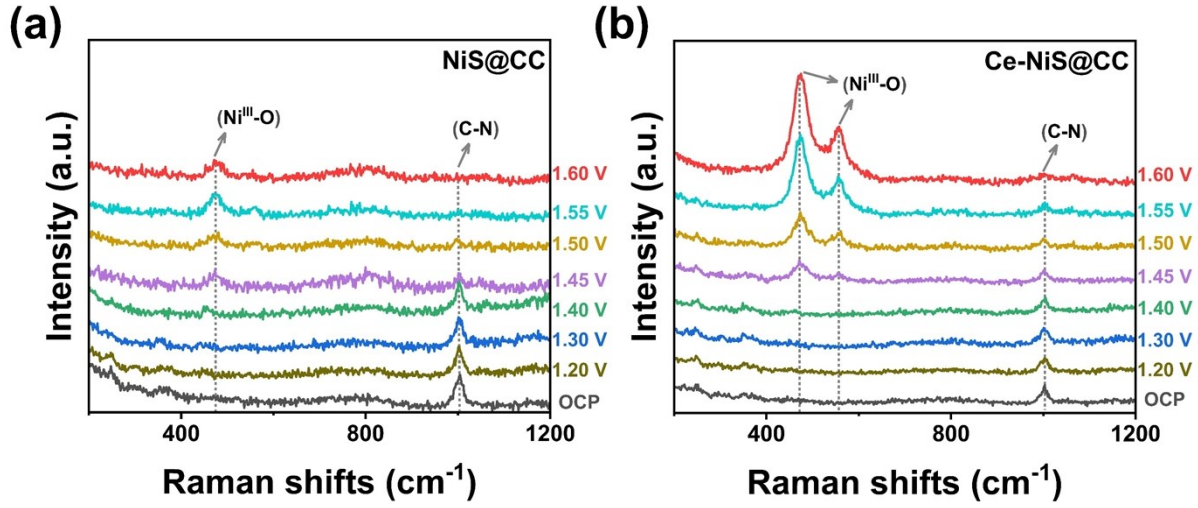

Figure S16. *In-situ* Raman spectra of (a) NiS and (b) Ce-NiS were recorded from OCP to 1.6 V *vs.* RHE in 1.0 M KOH with 0.33 M urea solution.

Supplementary Table

Table S1. Comparison of the activities of different UOR electrocatalysts.

Catalyst	Electrolyte	*E* (V *vs.* RHE) @ 100 mA cm^{-2}	Electrode	Ref.
Ce-NiS	1 M KOH+ 0.33 M Urea	1.41	CC	**This work**
AC-$Co_2(OH)_3Cl$-V-0.1	1M KOH+ 0.33 M Urea	1.62	No support	Chem. Eng. J., 2022, 439, 135768
NCVS-3	1 M KOH+ 0.33 M Urea	1.54	CP	ACS Catalysis, 2022, 12 (1), 569-579
$NiWO_4$-TA_{950}@Pt/C	1 M KOH+ 0.50 M Urea	1.49	CP	Energy Environ. Sci., 2022, 15, 2386-2396
Ovac-V-$Ni(OH)_2$	1M KOH+ 0.33 M Urea	1.47	NF	Adv. Funct. Mater., 2023, 33, 2209698
N-NiS/NiS_2	1M KOH+ 0.33 M Urea	1.47	CC	Chem. Eng. J., 2020, 397, 125507
NiFe/NiFeCH/CC	1M KOH+ 0.50 M Urea	1.44	CC	Nanoscale., 2023, 15, 779-790
Fc-NiCo-BDC	1M KOH+ 0.33 M Urea	1.44	NF	Chem. Eng. J., 2022, 430, 132733
W-NT@NF	1M KOH+ 0.33 M Urea	1.43	NF	Adv. Funct. Mater., 2023, 33, 2310155
NF/NiMoO	1M KOH+ 0.50 M Urea	1.42	NF	Energy Environ. Sci., 2018, 11, 1890-1897
Ni-WOx	1M KOH+ 0.33 M Urea	1.40	NF	Angew. Chem. Int. Ed., 2021, 60, 10577

Note: CC, CP, NF, GCE, and SiO_2 NM were stand for carbon cloth, carbon paper, nickel foam, glassy carbon electrode, and SiO_2 nanofibrous membrane, respectively.

Table S2. Comparison of the hydrogen production efficiency of different electrocatalysts in small molecule oxidation reaction coupled with HER, in the field of electrocatalysis (EC) and photocatalysis (PC).

Catalyst	Reaction	Hydrogen Production Rate	Field	Ref.
Ce-NiS	UOR-HER	75.73 μmol h^{-1}	EC	**This work**
	OER-HER	47.52 μmol h^{-1}		
$Ni(OH)_2$-SDS	ChOR-HER	90.0 μmol h^{-1}	EC	Nat. Commun., 2022, 13 (13), 5009
CoS@NiCu	AOR-HER	41.9 μmol h^{-1}	EC	Nano Energy, 2023, 117, 108896
$H_6[PV_3Mo_9O_{40}]$	GOR-HER	5.3 μmol C^{-1}	EC	Angew. Chem. Int. Ed., 2023, 62 (30), e202305843
TiO_2	MOR-HER	13.5 μmol h^{-1}	PC	Nat. Mater., 2023, 22 (5), 619-626
Pt NWs/C	EtOR-HER	1 mg h^{-1}	PC	Adv. Funct. Mater., 2020, 30 (49) 2004310

Note: UOR, ChOR, AOR, MOR, EtOR, GOR and HER were stand for urea oxidation reaction, cyclohexanone oxidation reaction, ammonia oxidation reaction, methanol oxidation reaction, ethanol oxidation reaction, glucose oxidation reaction and hydrogen evolution reaction, respectively.

References

1. B. Zhang, X. Zheng, O. Voznyy, R. Comin, M. Bajdich, M. García-Melchor, L. Han, J. Xu, M. Liu, L. Zheng, F. P. García de Arquer, C. T. Dinh, F. Fan, M. Yuan, E. Yassitepe, N. Chen, T. Regier, P. Liu, Y. Li, P. De Luna, A. Janmohamed, H. L. Xin, H. Yang, A. Vojvodic and E. H. Sargent, *Science*, 2016, **352**, 333-337.

2. Z. Ma, H. Wang, H. Ma, S. Zhan and Q. Zhou, *Fuel*, 2022, **315**, 123279.

3. Y. Zhang, Y. Lei, Y. Yan, W. Cai, J. Huang, Y. Lai and Z. Lin, *Appl. Catal., B*, 2024, **353**, 124064.

4. Z. Ma, H. Wang, H. Ma, S. Zhan and Q. Zhou, *Fuel*, 2022, **315**, 123279.

5. S. Zhan, Z. Zhou, M. Liu, Y. Jiao and H. Wang, *Catal. Today*, 2019, **327**, 398-404.

6. W. Yan, D. Wang, L. A. Diaz and G.G. Botte, *Electrochim. Acta*, 2014, **134**, 266-271.

7. S. Jeong, H. D. Mai, T. K. Nguyen, J.S. Youn, K.H. Nam, C.M. Park and K.J. Jeon, *Appl. Catal., B.*, 2021, **293**, 120227.

8. S. Sheng, K. Ye, Y. Gao, K. Zhu, J. Yan, G. Wang and D. Cao, *J. Colloid Interf. Sci.*, 2021, **602**, 325-333.

9. S. Niu, S. Li, Y. Du, X. Han and P. Xu, *ACS Energy Lett.*, 2020, **5**, 1083-1087.